ACS OMEGA

Article

Cite This: ACS Omega 2019, 4, 5275−5282

http://pubs.acs.org/journal/acsodf

Synthesis and Characterization of an SWCNT@HKUST-1 Composite: Enhancing the CO_2 Adsorption Properties of HKUST-1

Jonathan Cortés-Súarez,[†] Vanessa Celis-Arias,[†] Hiram I. Beltrán,[†] Adriana Tejeda-Cruz,[‡] Ilich A. Ibarra,*[,§] Josué E. Romero-Ibarra,[‡] Elí Sánchez-González,*[,§] and Sandra Loera-Serna*[,†]

[†]Departamento de Ciencias Básicas, Universidad Autónoma Metropolitana-Azcapotzalco, Av. San Pablo 180, Azcapotzalco, 02200 Ciudad de México, Mexico

[‡]Instituto de Investigaciones en Materiales and [§]Laboratorio de Fisicoquímica y Reactividad de Superficies (LaFReS), Instituto de Investigaciones en Materiales, Universidad Nacional Autónoma de México, Circuito Exterior s/n, CU, Coyoacán, 04510 Ciudad de México, Mexico

Supporting Information

ABSTRACT: Synthesis of a new HKUST-1 composite based on single-walled carbon nanotubes (SWCNTs) was successfully achieved (SWCNT@HKUST-1). SWCNTs were used as templates to grow rod-like HKUST-1 crystals over the surface of the nanotubes. N_2 adsorption properties showed an increment on the surface area and pore volume for the SWCNT@HKUST-1 composite. Furthermore, the CO_2 capture increased, from 7.92 to 8.75 mmol g^{-1} at 196 K up to 100 kPa, for the SWCNT@HKUST-1 composite. This enhancement was directly associated with the increase of the surface area of the composite. Additionally, an increase in the CO_2 heat of adsorption was estimated, from 30 to 39.1 kJ mol^{-1} for the SWCNT@HKUST-1 composite. In situ Raman experiments corroborated the favored CO_2 adsorption for the composite and provided an insight into the augmented hydrophobicity of the SWCNT@HKUST-1. Ethanol adsorption isotherms corroborated an increase in the hydrophobicity of the material upon the incorporation of carbon nanotubes.

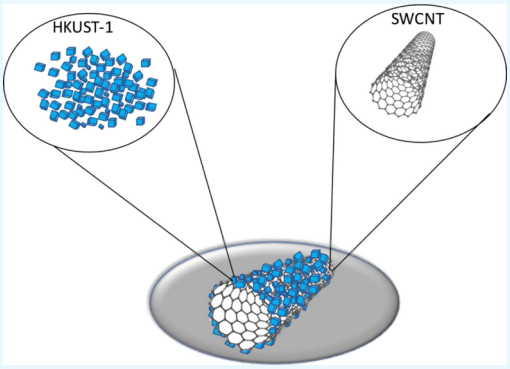

INTRODUCTION

One of the most studied and cited metal−organic framework (MOF) materials is, undoubtedly, HKUST-1 (HKUST = Hong Kong University of Science and Technology). HKUST-1, $[Cu_3(BTC)_2(H_2O)_3]_n$ (BTC = benzene-1,3,5-tricarboxylate), was first reported in 1999, and it is constructed by Cu_2 paddlewheel clusters connected by BTC^{3-} ligands, forming a cF crystal structure with $Fm\bar{3}m$ symmetry.[1] Its rigid porous open-framework exhibits bimodal pore size distribution and under the suitable activation conditions, it is possible to access the unsaturated metal sites [open metal sites (OMS)],[2,3] as water molecules can be removed to leave free sites in capped-octahedral Cu(II) metal ions. HKUST-1 has been demonstrated to be a promising MOF material in a large number of applications[4−6] because of its high surface area and the accessibility to OMS. Among these, energy-related applications (from energy storage to transformation) hold the most studied and interesting research-field for HKUST-1.[7] Indeed, it has been previously shown that access to the free coordination Cu(II) metal centers has considerably enhanced the gas adsorption properties of HKUST-1.[8,9] For example, by thoroughly integrating X-ray diffraction (XRD), extended X-ray absorption fine structure, UV−vis, X-ray absorption near-edge spectroscopy, and Raman spectroscopies, Bordiga[10] has demonstrated that by removing coordinated water molecules, chemically bound to the Cu(II) sites, the oxidation state of copper remained unaffected, the crystallinity of the material was maintained, and the gas adsorption properties enhanced. Thus, when HKUST-1 is activated to remove coordinated water molecules, a post-synthetic modification of the MOF material is achieved.

Another interesting strategy to enhance the adsorption properties of HKUST-1 is via its functionalization (modification). For example, the incorporation of different functional groups within the micropores of HKUST-1 has demonstrated superior CO_2 capture properties.[11,12] Another example of functionalization is the fabrication of composites (hybrid functionalized materials) using MOF materials and other crystalline structures, such as graphene or multiwalled carbon nanotubes. These examples have been previously reported, emphasizing on the adsorption of methane, benzene, ethanol, and other molecules.[13,14] In addition, the synthesis of composites based on carbon nanotubes and MOFs have shown promising results in the field of gas storage and in an ideal scenario, such composites would show an improved thermal conductivity in comparison to the pure MOF system (generally

Received: February 5, 2019
Accepted: March 1, 2019
Published: March 13, 2019

DOI: 10.1021/acsomega.9b00330
ACS Omega 2019, 4, 5275−5282

poor thermally conductive material). For example, Prasanth et al.[15] reported the synthesis of SWCNTs incorporated in MIL-101 to obtain a composite MOF material (SWNT@MIL-101), where the structure of the MOF material was not disturbed by the incorporation of SWCNTs. Hydrogen (H_2) adsorption capacities of MIL-101 were observed to be increased from 6.37 to 9.18 wt % at 77 K and 60 bar, and from 0.23 to 0.64 wt % at 298 K and 60 bar. Interestingly, the preparation of composites based on HKUST-1 is an active and attractive research area,[16,17] and thus, new and remarkable examples have shown exciting applications (e.g., H_2 storage, catalysis, chromatography, CO_2 capture, and lithium−sulfur batteries).[43,45,47,52−54]

Motivated by the remarkable results by Furukawa and other research groups,[18−22] we have synthesized and fully characterized an SWCNT-HKUST-1 composite (SWCNT@HKUST-1, see Scheme 1). We are interested in synthesizing composite adsorbent MOF materials capable to capture high amounts of CO_2 in parallel with our previous studies on H_2 storage.[23−25] Thus, in this contribution we show for the first time, to the best of our knowledge, the synthesis and characterization of a composite material based on SWCNTs and HKUST-1 entitled SWCNT@HKUST-1, along with its enhanced CO_2 adsorption properties.

Scheme 1. Synthetic Strategy for SWCNT@HKUST-1[a]

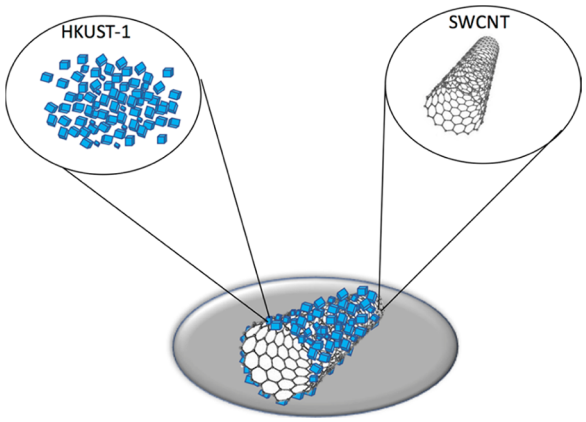

[a]HKUST-1 synthesis consists of the dropwise addition of a copper ethanolic solution into an aqueous solution of the deprotonated ligand, affording cuboctahedral crystals. When the SWCNTs are added into the mixture, the SWCNT@HKUST-1 composite is obtained.

EXPERIMENTAL SECTION

Chemicals. Benzene-1,3,5-tricarboxylic acid (H_3BTC, 95%), copper nitrate trihydrate (99.99%), nitric acid (70%), sodium bicarbonate (>99.7%), and sulfuric acid (98%) were purchased from Sigma-Aldrich and used as received. Anhydrous ethanol (99%, Aldrich) and deionized water were used as solvents. The SWCNTs (≥90%) were obtained from Sigma-Aldrich with a narrow diameter of 0.83 nm and were used for the preparation of the SWCNT@HKUST-1 composite material. Ultrapure grade (99.9995%) N_2 and CO_2 gases were obtained from Praxair.

Synthesis of HKUST-1. HKUST-1 was synthesized as reported by Loera-Serna et al.[25] Quantities of 2.38 mmol of H_3BTC and 7.14 mmol of $NaHCO_3$ (1:3 ratio) were dissolved in 150 mL of deionized water. Then, a solution which contains 3.57 mmol of copper nitrate trihydrate (3:2 $Cu(NO_3)_2$/H_3BTC ratio) and 40 mL of ethanol was added dropwise, and the reaction mixture was stirred at room temperature for 12 h. The obtained HKUST-1 product was isolated by centrifugation and dried at 323 K for 2 h, with a 89.6% yield in dry basis.

Functionalization of SWCNTs. The SWCNTs were functionalized before the composite synthesis. SWCNTs were mixed in a concentrated acid solution (3:1 H_2SO_4/HNO_3 ratio), and the reaction mixture was stirred at 353 K for 24 h. The functionalized SWCNTs were recovered by filtration, washed with deionized water, and dried at 353 K for 24 h.[26]

Synthesis of the SWCNT@HKUST-1 Composite. The functionalized SWCNTs were added in situ during the synthesis of HKUST-1 along with the raw materials to synthesize the SWCNT@HKUST-1 composite material. Different amounts of functionalized SWCNTs were used, 2, 5, and 10 wt %.

General Characterization. Powder X-ray diffraction patterns were collected on a Rigaku diffractometer, Ultima IV with a Cu Kα1 radiation (λ = 1.5406 Å) using a nickel filter. Patterns were recorded in the 5−60° 2θ range with a step scan of 0.02° and a scan rate of 0.1° min^{-1}. Thermogravimetric analyses (TGA) were performed in a TA Instruments Thermobalance, Q500 HR under N_2 atmosphere using the Hi-Res mode with a maximum rate of 5 K min^{-1} (sensitivity 1, resolution 5), from room temperature to 1073 K. Scanning electron microscopy micrographs were collected using a JEOL Benchtop Microscope, Neoscope JCM-6000. Transmission electron microscopy (TEM) micrographs were collected using a JEOL microscope, JEM-ARM200F; image processing was carried out in the DigitalMicrograph software form Gatan.

Raman Spectroscopy Experiments. The Raman spectra were collected using a Nicolet Almega XR-dispersive Raman spectrometer from Thermo Scientific; samples were excited with a focused green laser beam (λ = 523 nm). As-synthesized HKUST-1 and the SWCNT@HKUST-1 composite were measured at room temperature. The CO_2-loaded samples were activated prior to measurement; activation was carried out in a quartz tube at 393 K for 1 h; samples were cooled down to room temperature to acquire the spectra.

Adsorption Isotherms for N_2, CO_2, and EtOH. N_2 isotherms (up to P/P_0 = 1 and 77 K) were recorded on a BELSORP mini II analyzer under high vacuum in a clean system with a diaphragm pumping system. CO_2 isotherms (up to 1 bar and 196 K) were recorded on a BELSORP HP (high-pressure) analyzer. Prior to measurement samples were activated under vacuum (0.1 Pa) at 393 K for 1 h. Ethanol isotherms were measured at 303 K by a gravimetric method in a DVS Advantage 1 apparatus from Surface Measurement System, UK. This instrument consists of a Cahn microbalance (mass sensitivity: 0.1 μg), with a digital optical microscope, set up in an exactly controlled temperature and vapor pressure chamber (accuracy: 0.1 K and 0.7% P/P_0; respectively). Dry, and high-purity nitrogen was used as the carrier gas.

RESULTS AND DISCUSSION

Powder X-ray diffraction (PXRD) patterns of the HKUST-1 and 5 wt % SWCNT@HKUST-1 samples are compared in Figure 1; comparison of all different SWCNTs' loading is presented in Figure S2. All the diffraction peaks have been thoroughly indexed as cubic crystalline HKUST-1, corroborating that the MOF structure was not affected by the incorporation of SWCNTs. The cell parameters, determined

DOI: 10.1021/acsomega.9b00330
ACS Omega 2019, 4, 5275−5282

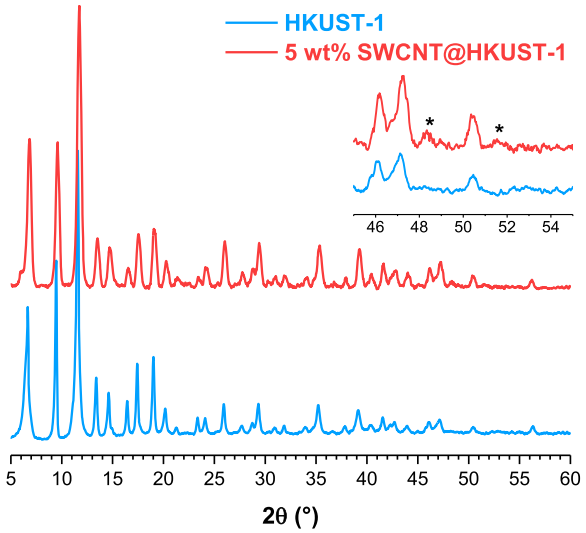

Figure 1. PXRD patterns of the HKUST-1 and 5 wt % SWCNT@HKUST-1 samples; the inset shows the SWCNT characteristic peaks.

in the (731) peak, were 26.27 and 26.14 Å for HKUST-1 and 5 wt % SWCNT@HKUST-1, respectively. The cell parameter value of the synthesized HKUST-1 is lower compared to that already reported for HKUST-1 (26.343 Å).[1] These results suggest that the synthetic procedures employed herein provided materials with a slightly compacted cell in comparison with solely HKUST-1, possibly due to the absence of solvent molecules in the pores of HKUST-1.

The reported HKUST-1 structure comprises three different cavities, with the capability of interconnecting pores within the net, thus forming channels. The largest channel shows, vertex to vertex (of the cuboctahedral cavity), Cu−OH_2···H_2O−Cu distances of 19.88 Å. The second one exhibits Cu···Cu distances of 18.62 Å. Meanwhile, the smallest channel shows COO···COO distances of 15.89 Å.[6] This suggests that HKUST-1 does not exhibit enough space to host SWCNT within its channels. A more plausible scenario is where SWCNTs could serve as a growing template or a crystallization seed for the HKUST-1. This type of templated growth has been reported in several nanostructures coated with MOFs, for different applications.[41−51] The difference between the crystal morphology of the HKUST-1 (cuboctahedron) with the thin rod crystals of the 5 wt % SWCNT@HKUST-1 (see Figure S3) points to this templated growth.

SWCNT characteristic reflections were identified in the PXRD pattern of the 5 wt % SWCNT@HKUST-1 sample, at 45.2° and 51.7° (2θ). It should be emphasized that XRD only detects crystalline compounds when the crystallite content is above ca. 3.0%.[3,27,28] Thus, SWCNTs should be present in a concentration of ca. 3.0%, in order to be identified by PXRD. An approximate amount of SWCNT 4.5% was estimated (comparing relative intensities from the PXRD experiment) in the 5 wt % SWCNT@HKUST-1 sample. This was made by using a differential intensity analysis of all diffracted peaks, considering that the two main peaks of SWCNT (at 45.2° and 51.7°) have different intensities in comparison to HKUST-1.

Table 1 summarizes the principal physicochemical (crystallographic) results of the synthesized HKUST-1 and 5 wt % SWCNT@HKUST-1, which are:

(a) The smaller intensity ratio of I_{222}/I_{422} reveals high electronic density content in X → Cu sites and thus the presence of carbon nanotubes in the outer or interaction surface instead of MOF cavities, as stated in Table 1.

(b) The small diffraction reflection at 5.9° (2θ) which corresponds to the (111) reflection, where this variation has been also observed in a previous contribution,[6] that could be associated with the absence of solvent molecules in the HKUST-1 pores.

(c) The elemental analysis of HKUST-1 and SWCNT@HKUST-1 was also determined by Energy-Dispersive X-Ray Spectroscopy (EDX); the difference in copper content was 39.94%. These determinations were made by averaging the EDXs of 10 different zones in the micrographs of each material. The elemental analysis shows a consistent increase in the percentage of carbon in the SWCNT@HKUST-1 composite because of the presence of the SWCNTs.

Table 1. Structural Parameters of HKUST-1 and SWCNT@HKUST-1

material	a_0 Å	D nm	I_{200}/I_{220}	% of carbon
HKUST-1	26.67	26.93	0.65	70.03 ± 0.59
SWCNT@HKUST-1	26.14	19.04	1.04	74.45 ± 6.51

The thermal stability of HKUST-1 and the 5 wt % SWCNT@HKUST-1 composite was investigated by TGA (Figure S1). The weight loss at temperatures lower than 398 K was attributed to the loss of weakly bound guest water molecules (desolvation of the structure), 34.94 and 25.98% for HKUST-1 and 5 wt % SWCNT@HKUST-1, respectively. Also, in the weight derivative it is observed that the desolvation of the 5 wt % SWCNT@HKUST-1 composite occurs at a lower temperature in comparison to the HKUST-1. This result suggests that the composite is more hydrophobic than the HKUST-1 because of the hydrophobic nature of the SWCNT. From 373 to 500 K weight losses of 32.11 and 41.09% were observed for HKUST-1 and 5 wt % SWCNT@HKUST-1, respectively, attributed to the BTC decomposition. Therefore, the thermal stability of the HKUST-1 decreased 46.7 K by incorporating SWCNT.

TEM images are shown in Figure 2, exhibiting the dimensions of the HKUST-1 crystal ranging from ca. 10 to 50 nm. The cubic symmetry of the HKUST-1 is also reflected in the shape of the crystals (Figure 2a). TEM images of the SWCNT@HKUST-1 composite material pointed that the SWCNTs are indeed well incorporated with HKUST-1 (Figure 2b). Actually, SWCNTs function as templates where microcrystals of HKUST-1 grow on top of their surface. This can be observed on the TEM image at low magnification (Figure 2b). Thus, TEM micrographs suggest that SWCNTs were not inside the pores of the HKUST-1 as expected.[29] Black spots appear in the edges of the HKUST-1 crystals. This is due to their sensitivity to the electron beam and, under standard experimental conditions, the copper oxide is formed after only few minutes, as it has been shown for similar systems,[29] Figure 2b.

The high-resolution images of the composite (Figure 2c) also show two distinctive lattice spacings of 6.3 and 9.06 Å, which correspond to the interlayer spacing values for the (400) and (220) planes of HKUST-1. These planes were identified by their selected area electron diffraction (Figure 2d,e). No evidence was found of SWCNTs on the surface of the composite. It was assumed that the HKUST-1 crystals were formed by heteronucleation. This might be due to the growth

DOI: 10.1021/acsomega.9b00330
ACS Omega 2019, 4, 5275−5282

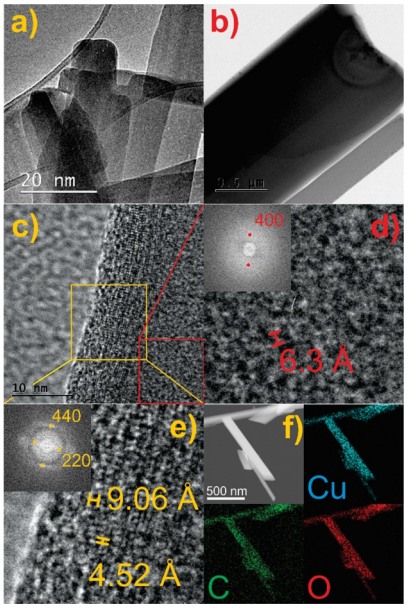

Figure 2. TEM images of (a) HKUST-1 and SWCNT@HKUST-1 at (b) low magnification and (c) high magnification, (d,e) selected area electron diffraction for the SWCNT@HKUST-1 composite, and (f) elemental mapping (blue: copper; green: carbon; red: oxygen) of the SWCNT@HKUST-1 composite.

of HKUST-1 on the surface of the functional groups on SWCNTs, leading to the growth of the MOF on the outside of the tubes. However, it was very difficult to characterize the interface region between the SWCNTs and the MOF by using available techniques. Nonetheless, long crystals were obtained for the SWCNT@HKUST-1 composite, a nontypical HKUST-1 crystal habit which hint a templated growth, where the composite retains the SWCNT rod-like shape (Figure 2f). The width of these rod-like crystals varies from 170 to 350 nm (Figure S4); thus, a nanometric size composite (SWCNT@HKUST-1) was obtained.

In order to determine the SWCNT incorporation on the SWCNT@HKUST-1 composite, Raman experiments were carried out (Figures 3 and S7). Interestingly, the characteristic

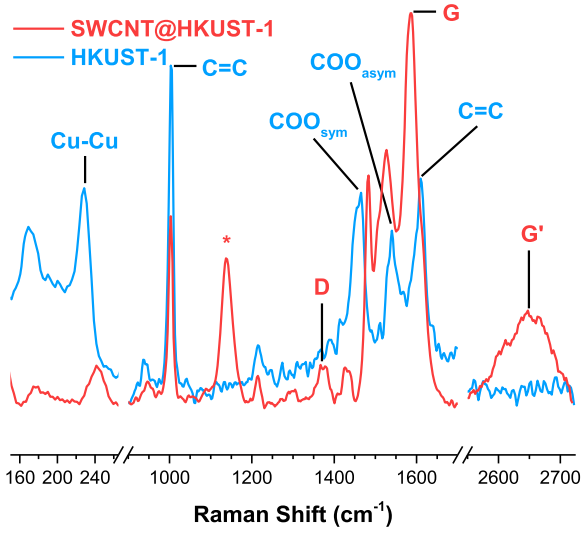

Figure 3. Raman spectra for HKUST-1 and 5 wt % SWCNT@HKUST-1, highlighting the SWCNT bands.

stretching vibration modes of the carbon nanotubes were clearly observed, see Figure 3. Raman shift for the D-, G-, and G′-bands for the SWCNTs were observed in the Raman spectra, at 1370, 1586, and 2650 cm^{-1}, respectively (see Figure 3).[30] An additional band found at 1137 cm^{-1} can be associated with surface-modified SWCNTs with COO-attached groups.[31] Typical HKUST-1 Raman peaks were identified in both samples (Figure 3).[10,32,33] Bands associated with the C═C modes form the benzene ring that appeared at 1003 and 1610 cm^{-1}; the latter appeared as a shoulder next to the G-band from the SWCNTs in the SWCNT@HKUST-1 composite spectra. Symmetric and asymmetric −COO modes form the carboxylates that appeared at 1460 and 1540 cm^{-1}, respectively. SWCNT@HKUST-1 signals red-shifted to 1427 and 1527 cm^{-1}. Copper OMS can be difficult to observe because of the hygroscopic nature of these sites. Both H_2O-coordinated and OMS bands are observed at 169 and 228 cm^{-1} respectively;[34−36] for the SWCNT@HKUST-1 composite this H_2O-coordinated peak is relatively smaller than the OMS peak because of a more hydrophobic nature of the composite.

The textural homogeneity of HKUST-1 and the SWCNT@HKUST-1 composites is reflected on the nitrogen adsorption isotherms presented in Figure 4. They have a well-defined

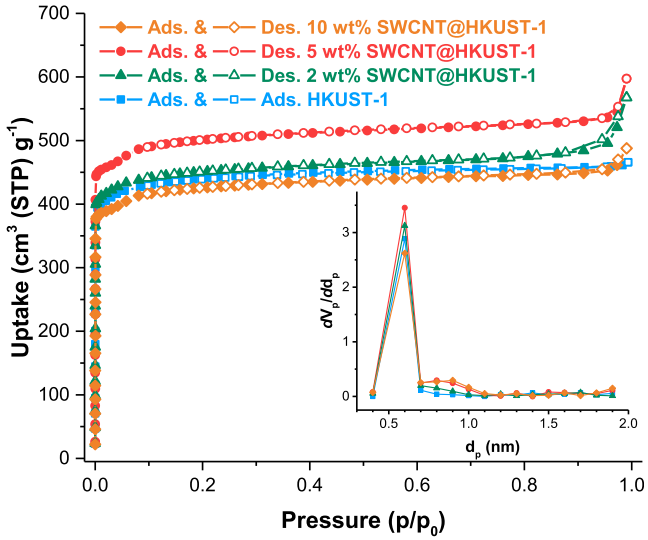

Figure 4. HKUST-1 and SWCNT@HKUST-1 composites' N_2 adsorption isotherms at 77 K; the inset shows the micropore distribution of each sample.

type-I shape indicating microporosity and pores with a uniform size, which agrees with the structure of HKUST-1. From these isotherms, the parameters of the porous structures were calculated and are presented in Table 2. The composite with 5 wt % SWCNT has ca. 20% higher surface area and pore volume than HKUST-1. The sample with 2 wt % of SWCNT shows a little increase in the surface area, with respect to the HKUST-1. Conversely, the sample with 10 wt % SWCNT showed a decrease in the surface area. It is worth to mention that the mechanical mixture of HKUST-1 and SWCNT in the same proportion to the composite (vide supra, Experimental Section) did not show any enhanced surface area. These results suggest that HKUST-1 particles are well dispersed on the SWCNT surface, increasing the accessible area. The difference between pore diameters is less evident than the surface areas

DOI: 10.1021/acsomega.9b00330
ACS Omega 2019, 4, 5275−5282

Table 2. Selected Adsorption Properties for the HKUST-1 and SWCNT@HKUST-1 Composites

material	$S_{a,BET}$ $m^2\ g^{-1}$	V_{pore} $cm^3\ g^{-1}$	D_{pore} nm	n_{ads} (CO_2) mmol g^{-1}	Q_{st} (CO_2) kJ mol^{-1}
HKUST-1	1410	0.7053	0.64	7.92	30[37]
2 wt % SWCNT@HKUST-1	1520	0.7512	0.64	8.23	
5 wt % SWCNT@HKUST-1	1714	0.9203	0.67	8.75	39.1
10 wt % SWCNT@HKUST-1	1370	0.6891	0.62	7.73	

and pore volumes. The pore distribution shows a marked difference around 0.8−0.9 nm (inset Figure 4), where the SWCNT@HKUST-1 composites show a local maximum. This may be associated with the presence of the SWCNTs with a diameter of ca. 0.83 nm.

CO_2 adsorption isotherms at 196 K were measured for all materials (Figure 5). HKUST-1 and SWCNT@HKUST-1

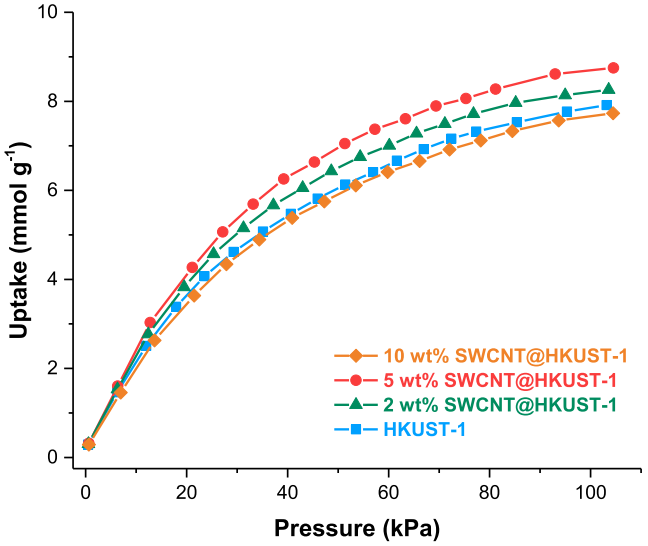

Figure 5. HKUST-1 and SWCNT@HKUST-1 composites' CO_2 adsorption isotherms at 196 K.

composites were activated prior to measurements at 393 K for 1 h, vide supra. HKUST-1 adsorbed a total amount of 7.92 mmol g^{-1} of CO_2. An enhanced CO_2 adsorption was observed for the 2 and 5 wt % SWCNT@HKUST-1 composite with 8.23 and 8.75 mmol g^{-1}, respectively. This can be explained by the augment in the surface area provided by the incorporation of the SWCNTs, although when a 10 wt % load is reached, the CO_2 uptake does not show any improvement. Additionally, CO_2 adsorption isotherms were carried out at 213 and 231 K for the 5 wt % SWCNT@HKUST-1 material to estimate the isosteric heat of adsorption (see the Supporting Information). The 5 wt % SWCNT@HKUST-1 CO_2 isosteric heat of adsorption (39.1 kJ mol^{-1}) was greater than that reported for the HKUST-1 (30 kJ mol^{-1}).

The adsorption of CO_2 in HKUST-1 and 5 wt % SWCNT@HKUST-1 was investigated by in situ Raman experiments (Figure 6). The samples were activated in a quartz cell prior to the experiments, vide supra. First, the analysis on HKUST-1 demonstrated the characteristic Cu−Cu vibration band at 228 cm^{-1} (from the copper paddlewheel) red-shifted to 216 cm^{-1}

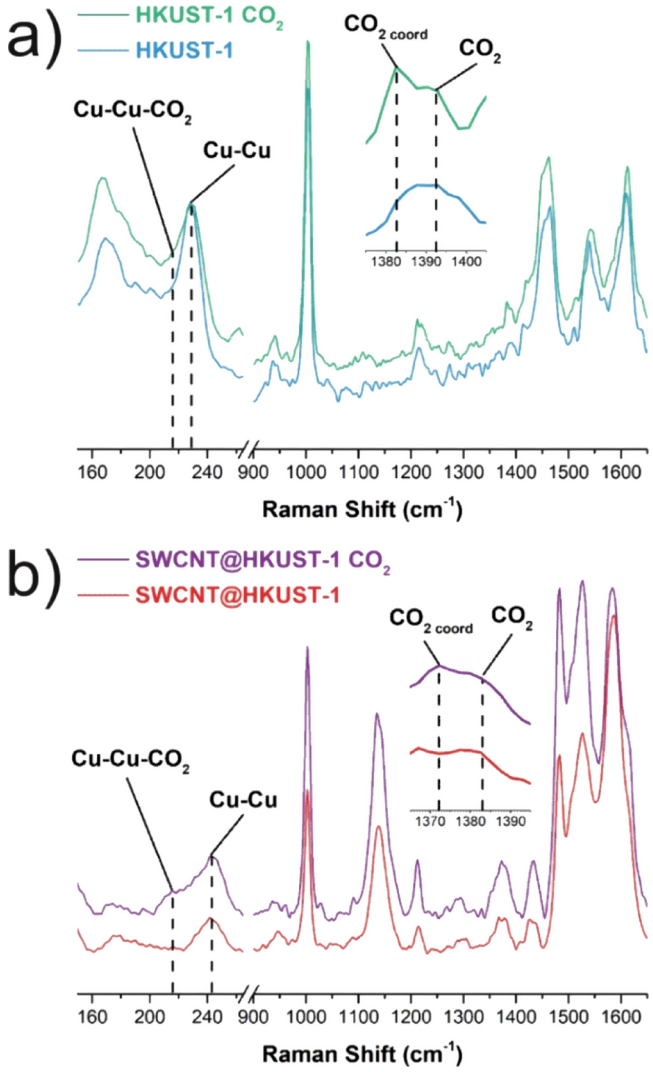

Figure 6. Raman spectra for (a) HKUST-1 and (b) 5 wt % SWCNT@HKUST-1, before and after CO_2 adsorption.

upon CO_2 adsorption (see Figure 6a). Despite the HKUST-1 sample being activated and then exposed to pure CO_2 gas, the characteristic band associated with the interaction Cu−Cu−CO_2 (open metal site), at approximately 220 cm^{-1}, appeared as a small shoulder next to the characteristic band associated with OMS (Figure 6a). Although HKUST-1 was fully activated, the Raman spectra evidenced the presence coordinated water (because of the hygroscopic nature of HKUST-1), and it was observed in both spectra at 169 and 167 cm^{-1} (Figure 6a). These water molecules occupied the preferential adsorption sites and prevented CO_2 adsorption (small shoulder at 220 cm^{-1}).[38] In the case of the sample 5 wt % SWCNT@HKUST-1, the characteristic OMS vibration band was also found to be well defined at 242 cm^{-1}(Figure 6b), and a sharp band at 216 cm^{-1} corroborated the CO_2 adsorption in the composite (Figure 6b). The bands corresponding to coordinated water in 5 wt % SWCNT@HKUST-1, at 177 and 174 cm^{-1}, showed smaller intensities in comparison to HKUST-1. The characteristic H_2O-coordinated band red-shifted (approximately 2−3 cm^{-1}) in both materials (HKUST-1 and 5 wt % SWCNT@HKUST-1) when CO_2 is adsorbed. This shift suggests a small interaction between CO_2 and the coordinated water. A characteristic CO_2 Fermi

DOI: 10.1021/acsomega.9b00330
ACS Omega 2019, 4, 5275−5282

resonance band appeared at 1393 cm^{-1} for both samples (HKUST-1 and 5 wt % SWCNT@HKUST-1, see the inset of Figure 6). This can be attributed to free CO_2 molecules inside the measurement system. Interestingly, an additional band appeared upon the CO_2 adsorption at 1382 cm^{-1} for HKUST-1 (see the inset of Figure 6a). This was associated with CO_2 coordinated to HKUST-1, providing additional evidence of the relatively strong CO_2−MOF interaction.[38] Evidence of the CO_2 coordination with the 5 wt % SWCNT@HKUST-1 was also found at 1372 cm^{-1} (see the inset of Figure 6b).

Finally, evidence of increased hydrophobicity for the composite (SWCNT@HKUST-1) was suggested by our Raman spectroscopy results. As HKUST-1 is water-unstable, ethanol (EtOH) sorption experiments were selected to investigate such hydrophobicity. We have previously demonstrated that HKUST-1 was stable toward this polar solvent (EtOH),[39] and provided us the guideline to investigate the hydrophobicity of the composite (SWCNT@HKUST-1). Then, the EtOH adsorption for HKSUT-1 showed a total of 54.6 wt % uptake, which decreased (to 49.2 wt %) upon SWCNT inclusion (see Figure 7, HKUST-1 and SWCNT@HKUST-1 EtOH uptakes). The EtOH adsorption isotherm for HKUST-1exhibited a steep increase at low P/P_0 values, reaching saturation at 10 P/P_0 (see Figure 7). Such a rapid EtOH uptake suggests a strong affinity for EtOH. Conversely, the EtOH adsorption for SWCNT@HKUST-1 showed a considerably less steeped uptake increase and the saturation point was shifted to greater P/P_0 values (20 P/P_0), see Figure 7, indicating a reduced affinity for EtOH. These results demonstrate an enhanced hydrophobicity for the SWCNT@HKUST-1 composite.

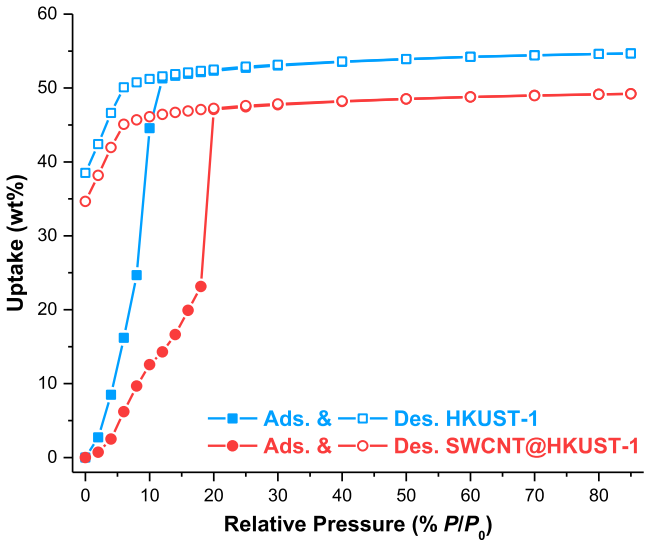

Figure 7. Ethanol adsorption−desorption isotherms at 303 K for HKUST-1 and 5 wt % SWCNT@HKUST-1.

Raman experiments can be correlated with the observed adsorption properties. The evidence of CO_2 molecules coordinated to the OMS in both materials (Figure 6) gave us an insight on the level of interaction between CO_2 and the OMS. The signal ratios for the Cu−Cu−CO_2 (220 cm^{-1}) and Cu−Cu (240 cm^{-1}) bands are higher for the SWCNT@HKUST-1 composite. This observation can be interpreted as a strong CO_2 interaction with the composite in comparison to the bare HKUST-1. The heat of adsorption for CO_2 corroborates this hypothesis, 39.1 kJ mol^{-1} for SWCNT@HKUST-1 over 30 kJ mol^{-1} for HKUST-1; this increase can be associated with the shape of the rod-like crystals. The nanometric width of the crystals leads to a better access to the centers of these, where presumably the SWCNTs can be found and provide an extra CO_2 adsorption site.[40]

CONCLUSIONS

The synthesis of a new composite based on HKUST-1 and SWCNTs was successfully demonstrated. A comprehensive characterization set (PXRD, TGA, TEM, EDX, and Raman spectroscopy) for the composite 5 wt % SWCNT@HKUST-1 confirmed the growing of HKUST-1 on the surface of SWCNTs and the nanosize of the composite. N_2 adsorption isotherms corroborated a higher surface area and pore volume for 5 wt % SWCNT@HKUST-1 than HKUST-1. These results suggested that HKUST-1 particles are well dispersed on the SWCNT surface, increasing the accessible area. A mechanical mixture of HKUST-1 and SWCNTs in the same proportion to the composite (Experimental Section) did not show any enhanced surface area. This confirmed the chemical deposition of HKUST-1 on the surface of SWCNTs. CO_2 adsorption experiments, at 196 K, demonstrated an enhanced CO_2 capture for 5 wt % SWCNT@HKUST-1 (8.75 mmol g^{-1}) over HKUST-1 (7.92 mmol g^{-1}). Isosteric heat of adsorption for CO_2 was also estimated to be higher for the composite (form 30 kJ mol^{-1} for HKUST-1 to 39.1 kJ mol^{-1} for 5 wt % SWCNT@HKUST-1). In situ Raman spectroscopy revealed the preferential CO_2 adsorption sites on 5 wt % SWCNT@HKUST-1, corroborated its higher CO_2 heat of adsorption, and evidenced the augmented hydrophobicity of the composite. Finally, such hydrophobicity of the composite was investigated by the adsorption of ethanol vapor, finding a reduced affinity to EtOH in comparison to HKUST-1. Thus, 5 wt % SWCNT@HKUST-1 has demonstrated interesting properties which enlarge the research on MOF composites.[46,55]

ASSOCIATED CONTENT

Supporting Information

The Supporting Information is available free of charge on the ACS Publications website at DOI: 10.1021/acsomega.9b00330.

TGA data, TEM micrographs, EDX analysis, additional CO_2 adsorption isotherms, and heat of adsorption calculation (PDF)

AUTHOR INFORMATION

Corresponding Authors

*E-mail: argel@unam.mx. Fax: +52(55) 5622-4595 (I.A.I.).
*E-mail: kunikleto@comunidad.unam.mx (E.S.-G.).
*E-mail: sls@azc.uam.mx (S.L.-S.).

ORCID

Ilich A. Ibarra: 0000-0002-8573-8033
Elí Sánchez-González: 0000-0002-5440-329X
Sandra Loera-Serna: 0000-0001-9562-3195

Author Contributions

The article was written through contributions of all the authors. All the authors have given approval to the final version of the article.

DOI: 10.1021/acsomega.9b00330
ACS Omega 2019, 4, 5275−5282

Funding

CONACyT Mexico, grants: 1789, A1-S-31186, 154736 and 289042. PAPIIT-UNAM Mexico, grant: IN101517.

Notes

The authors declare no competing financial interest.

■ ACKNOWLEDGMENTS

The authors thank CONACyT Mexico (1789, A1-S-31186, 154736, and 289042), PAPIIT UNAM Mexico (IN101517) for financial support. Thanks are extended to U. Winnberg (ITAM) for scientific discussions.

■ REFERENCES

(1) Chui, S. S.; Lo, S. M.-F.; Charmant, J. P. H.; Orpen, A. G.; Williams, I. D. A Chemically Functionalizable Nanoporous Material $[Cu_3(TMA)_2(H_2O)_3]_n$. *Science* **1999**, *283*, 1148−1150.

(2) Hartmann, M.; Kunz, S.; Himsl, D.; Tangermann, O.; Ernst, S.; Wagener, A. Adsorptive Separation of Isobutene and Isobutane on $Cu_3(BTC)_2$. *Langmuir* **2008**, *24*, 8634−8642.

(3) Loera-Serna, S.; Oliver-Tolentino, M. A.; de Lourdes López-Núñez, M.; Santana-Cruz, A.; Guzmán-Vargas, A.; Cabrera-Sierra, R.; Beltrán, H. I.; Flores, J. Electrochemical behavior of $[Cu_3(BTC)_2]$ metal−organic framework: The effect of the method of synthesis. *J. Alloys Compd.* **2012**, *540*, 113−120.

(4) Furukawa, H.; Cordova, K. E.; O'Keeffe, M.; Yaghi, O. M. The Chemistry and Applications of Metal-Organic Frameworks. *Science* **2013**, *341*, 1230444.

(5) Yepez, R.; García, S.; Schachat, P.; Sánchez-Sánchez, M.; González-Estefan, J. H.; González-Zamora, E.; Ibarra, I. A.; Aguilar-Pliego, J. Catalytic activity of HKUST-1 in the oxidation of trans-ferulic acid to vanillin. *New J. Chem.* **2015**, *39*, 5112−5115.

(6) Celis-Arias, V.; Loera-Serna, S.; Beltrán, H. I.; Álvarez-Zeferino, J. C.; Garrido, E.; Ruiz-Ramos, R. The fungicide effect of HKUST-1 on Aspergillus niger, Fusarium solani and Penicillium chrysogenum. *New J. Chem.* **2018**, *42*, 5570−5579.

(7) Yoon, M.; Suh, K.; Natarajan, S.; Kim, K. Proton Conduction in Metal-Organic Frameworks and Related Modularly Built Porous Solids. *Angew. Chem., Int. Ed.* **2013**, *52*, 2688−2700.

(8) Wang, Q. M.; Shen, D.; Bülow, M.; Lau, M. L.; Deng, S.; Fitch, F. R.; Lemcoff, N. O.; Semanscin, J. Metallo-organic molecular sieve for gas separation and purification. *Microporous Mesoporous Mater.* **2002**, *55*, 217−230.

(9) Millward, A. R.; Yaghi, O. M. Metal−Organic Frameworks with Exceptionally High Capacity for Storage of Carbon Dioxide at Room Temperature. *J. Am. Chem. Soc.* **2005**, *127*, 17998−17999.

(10) Prestipino, C.; Regli, L.; Vitillo, J. G.; Bonino, F.; Damin, A.; Lamberti, C.; Zecchina, A.; Solari, P. L.; Kongshaug, K. O.; Bordiga, S. Local Structure of Framework Cu(II) in HKUST-1 Metallorganic Framework: Spectroscopic Characterization upon Activation and Interaction with Adsorbates. *Chem. Mater.* **2006**, *18*, 1337−1346.

(11) Jeong, N. C.; Samanta, B.; Lee, C. Y.; Farha, O. K.; Hupp, J. T. Coordination-Chemistry Control of Proton Conductivity in the Iconic Metal-Organic Framework Material HKUST-1. *J. Am. Chem. Soc.* **2011**, *134*, 51−54.

(12) Yazaydın, A. Ö.; Benin, A. I.; Faheem, S. A.; Jakubczak, P.; Low, J. J.; Willis, R. R.; Snurr, R. Q. Enhanced CO_2 Adsorption in Metal-Organic Frameworks via Occupation of Open-Metal Sites by Coordinated Water Molecules. *Chem. Mater.* **2009**, *21*, 1425−1430.

(13) Xiang, Z.; Hu, Z.; Cao, D.; Yang, W.; Lu, J.; Han, B.; Wang, W. Metal-Organic Frameworks with Incorporated Carbon Nanotubes: Improving Carbon Dioxide and Methane Storage Capacities by Lithium Doping. *Angew. Chem., Int. Ed.* **2011**, *50*, 491−494.

(14) Liu, G.-q.; Wan, M.-x.; Huang, Z.-h.; Kang, F.-y. Preparation of graphene/metal-organic composites and their adsorption performance for benzene and ethanol. *New Res. Carbon Mater.* **2015**, *30*, 566−571.

(15) Prasanth, K. P.; Rallapalli, P.; Raj, M. C.; Bajaj, H. C.; Jasra, R. V. Enhanced hydrogen sorption in single walled carbon nanotube incorporated MIL-101 composite metal-organic framework. *Int. J. Hydrogen Energy* **2011**, *36*, 7594−7601.

(16) Xu, F.; Yu, Y.; Yan, J.; Xia, Q.; Wang, H.; Li, J.; Li, Z. Ultrafast room temperature synthesis of GrO@HKUST-1 composites with high CO_2 adsorption capacity and CO_2/N_2 adsorption selectivity. *Chem. Eng. J.* **2016**, *303*, 231−237.

(17) Petit, C.; Bandosz, T. J. Exploring the coordination chemistry of MOF-graphite oxide composites and their applications as adsorbents. *Dalton Trans.* **2012**, *41*, 4027−4035.

(18) Khaletskaya, K.; Reboul, J.; Meilikhov, M.; Nakahama, M.; Diring, S.; Tsujimoto, M.; Isoda, S.; Kim, F.; Kamei, K.-i.; Fischer, R. A.; Kitagawa, S.; Furukawa, S. Integration of Porous Coordination Polymers and Gold Nanorods into Core-Shell Mesoscopic Composites toward Light-Induced Molecular Release. *J. Am. Chem. Soc.* **2013**, *135*, 10998−11005.

(19) Bradshaw, D.; Garai, A.; Huo, J. Metal-organic framework growth at functional interfaces: thin films and composites for diverse applications. *Chem. Soc. Rev.* **2012**, *41*, 2344−2381.

(20) Yang, Q.; Liu, W.; Wang, B.; Zhang, W.; Zeng, X.; Zhang, C.; Qin, Y.; Sun, X.; Wu, T.; Liu, J.; Huo, F.; Lu, J. Regulating the spatial distribution of metal nanoparticles within metal-organic frameworks to enhance catalytic efficiency. *Nat. Commun.* **2017**, *8*, 14429.

(21) Stock, N.; Biswas, S. Synthesis of metal-organic frameworks (MOFs): routes to various MOF topologies, morphologies, and composites. *Chem. Rev.* **2012**, *112*, 933−969.

(22) Mao, Y.; Li, J.; Cao, W.; Ying, Y.; Hu, P.; Liu, Y.; Sun, L.; Wang, H.; Jin, C.; Peng, X. General incorporation of diverse components inside metal-organic framework thin films at room temperature. *Nat. Commun.* **2014**, *5*, 5532.

(23) Ibarra, I. A.; Lin, X.; Yang, S.; Blake, A. J.; Walker, G. S.; Barnett, S. A.; Allan, D. R.; Champness, N. R.; Hubberstey, P.; Schröder, M. Structures and H_2 Adsorption Properties of Porous Scandium Metal-Organic Frameworks. *Chem.—Eur. J.* **2010**, *16*, 13671−13679.

(24) Ibarra, I. A.; Yang, S.; Lin, X.; Blake, A. J.; Rizkallah, P. J.; Nowell, H.; Allan, D. R.; Champness, N. R.; Hubberstey, P.; Schröder, M. Highly porous and robust scandium-based metal-organic frameworks for hydrogen storage. *Chem. Commun.* **2011**, *47*, 8304−8306.

(25) Loera-Serna, S.; Núñez, L. L.; Flores, J.; López-Simeon, R.; Beltrán, H. I. An alkaline one-pot metathesis reaction to give a $[Cu_3(BTC)_2]$ MOF at r.t., with free Cu coordination sites and enhanced hydrogen uptake properties. *RSC Adv.* **2013**, *3*, 10962−10972.

(26) Yang, S. J.; Choi, J. Y.; Chae, H. K.; Cho, J. H.; Nahm, K. S.; Park, C. R. Preparation and Enhanced Hydrostability and Hydrogen Storage Capacity of CNT@MOF-5 Hybrid Composite. *Chem. Mater.* **2009**, *21*, 1893−1897.

(27) Alvarez, L. J.; Ramírez-Solís, A.; Bosch Giral, P. Mechanisms of formation of extraframework Al_2O_3 in zeolites. *Zeolites* **1997**, *18*, 54−62.

(28) Loera, S.; Llewellyn, P. L.; Lima, E. Na^+ Charge Tuning through Encapsulation of Sulfur Chromophores in Zeolite A and the Consequences in Adsorbent Properties. *J. Phys. Chem. C* **2010**, *114*, 7880−7887.

(29) Lebedev, O. I.; Millange, F.; Serre, C.; Van Tendeloo, G.; Férey, G. First Direct Imaging of Giant Pores of the Metal−Organic Framework MIL-101. *Chem. Mater.* **2005**, *17*, 6525−6527.

(30) Saito, R.; Grüneis, A.; Samsonidze, G. G.; Brar, V. W.; Dresselhaus, G.; Dresselhaus, M. S.; Jorio, A.; Cançado, L. G.; Fantini, C.; Pimenta, M. A.; Filho, A. G. S. Double resonance Raman spectroscopy of single-wall carbon nanotubes. *New J. Phys.* **2003**, *5*, 157.

(31) Hussain, S.; Jha, P.; Chouksey, A.; Raman, R.; Islam, S. S.; Islam, T.; Choudhary, P. K.; Harsh. Spectroscopic Investigation of Modified Single Wall Carbon Nanotube (SWCNT). *J. Mod. Phys.* **2011**, *02*, 538−543.

(32) Petit, C.; Mendoza, B.; O'Donnell, D.; Bandosz, T. J. Effect of Graphite Features on the Properties of Metal-Organic Framework/

DOI: 10.1021/acsomega.9b00330
ACS Omega 2019, 4, 5275−5282

Graphite Hybrid Materials Prepared Using an in Situ Process. *Langmuir* **2011**, *27*, 10234−10242.
(33) Dhumal, N. R.; Singh, M. P.; Anderson, J. A.; Kiefer, J.; Kim, H. J. Molecular Interactions of a Cu-Based Metal-Organic Framework with a Confined Imidazolium-Based Ionic Liquid: A Combined Density Functional Theory and Experimental Vibrational Spectroscopy Study. *J. Phys. Chem. C* **2016**, *120*, 3295−3304.
(34) Kim, H. K.; Yun, W. S.; Kim, M.-B.; Kim, J. Y.; Bae, Y.-S.; Lee, J.; Jeong, N. C. A Chemical Route to Activation of Open Metal Sites in the Copper-Based Metal-Organic Framework Materials HKUST-1 and Cu-MOF-2. *J. Am. Chem. Soc.* **2015**, *137*, 10009−10015.
(35) Bae, J.; Choi, J. S.; Hwang, S.; Yun, W. S.; Song, D.; Lee, J.; Jeong, N. C. Multiple Coordination Exchanges for Room-Temperature Activation of Open-Metal Sites in Metal-Organic Frameworks. *ACS Appl. Mater. Interfaces* **2017**, *9*, 24743−24752.
(36) Choi, J. S.; Bae, J.; Lee, E. J.; Jeong, N. C. A Chemical Role for Trichloromethane: Room-Temperature Removal of Coordinated Solvents from Open Metal Sites in the Copper-Based Metal-Organic Frameworks. *Inorg. Chem.* **2018**, *57*, 5225−5231.
(37) Das, A.; D'Alessandro, D. M. Tuning the functional sites in metal−organic frameworks to modulate CO_2 heats of adsorption. *CrystEngComm* **2015**, *17*, 706−718.
(38) Chen, Y.; Wang, H.; Li, J.; Lockard, J. V. *In situ* spectroscopy studies of CO_2 adsorption in a dually functionalized microporous metal−organic framework. *J. Mater. Chem. A* **2015**, *3*, 4945−4953.
(39) Álvarez, J. R.; Sánchez-González, E.; Pérez, E.; Schneider-Revueltas, E.; Martínez, A.; Tejeda-Cruz, A.; Islas-Jácome, A.; González-Zamora, E.; Ibarra, I. A. Structure stability of HKUST-1 towards water and ethanol and their effect on its CO_2 capture properties. *Dalton Trans.* **2017**, *46*, 9192−9200.
(40) Rahimi, M.; Singh, J. K.; Babu, D. J.; Schneider, J. J.; Müller-Plathe, F. Understanding Carbon Dioxide Adsorption in Carbon Nanotube Arrays: Molecular Simulation and Adsorption Measurements. *J. Phys. Chem. C* **2013**, *117*, 13492−13501.
(41) Jahan, M.; Bao, Q.; Yang, J.-X.; Loh, K. P. Structure-Directing Role of Graphene in the Synthesis of Metal−Organic Framework Nanowire. *J. Am. Chem. Soc.* **2010**, *132*, 14487−14495.
(42) Ge, L.; Wang, L.; Rudolph, V.; Zhu, Z. Hierarchically structured metal−organic framework/ vertically-aligned carbon nanotubes hybrids for CO_2 capture. *RSC Adv.* **2013**, *3*, 25360−25366.
(43) Silvestre, M. E.; Franzreb, M.; Weidler, P. G.; Shekhah, O.; Wöll, C. Magnetic Cores with Porous Coatings: Growth of Metal-Organic Frameworks on Particles Using Liquid Phase Epitaxy. *Adv. Funct. Mater.* **2013**, *23*, 1210−1213.
(44) Zhang, W.; Wu, Z.-Y.; Jiang, H.-L.; Yu, S.-H. Nanowire-Directed Templating Synthesis of Metal-Organic Framework Nanofibers and Their Derived Porous Doped Carbon Nanofibers for Enhanced Electrocatalysis. *J. Am. Chem. Soc.* **2014**, *136*, 14385−14388.
(45) Li, G.; Kobayashi, H.; Taylor, J. M.; Ikeda, R.; Kubota, Y.; Kato, K.; Takata, M.; Yamamoto, T.; Toh, S.; Matsumura, S.; Kitagawa, H. Hydrogen storage in Pd nanocrystals covered with a metal-organic framework. *Nat. Mater.* **2014**, *13*, 802−806.
(46) Doherty, C. M.; Buso, D.; Hill, A. J.; Furukawa, S.; Kitagawa, S.; Falcaro, P. Using Functional Nano- and Microparticles for the Preparation of Metal-Organic Framework Composites with Novel Properties. *Acc. Chem. Res.* **2014**, *47*, 396−405.
(47) Toyao, T.; Styles, M. J.; Yago, T.; Sadiq, M. M.; Riccò, R.; Suzuki, K.; Horiuchi, Y.; Takahashi, M.; Matsuoka, M.; Falcaro, P. Fe_3O_4@HKUST-1 and Pd/Fe_3O_4@HKUST-1 as magnetically recyclable catalysts prepared via conversion from a Cu-based ceramic. *CrystEngComm* **2017**, *19*, 4201−4210.
(48) Qin, R.; Zeng, H. C. Design and Synthesis of Supported Nanoscale Metal-Organic Frameworks: Transformation from Transition Metal Silicates. *ACS Sustainable Chem. Eng.* **2018**, *6*, 14979−14988.
(49) Ellis, J. E.; Zeng, Z.; Hwang, S. I.; Li, S.; Luo, T.-Y.; Burkert, S. C.; White, D. L.; Rosi, N. L.; Gassensmith, J. J.; Star, A. Growth of ZIF-8 on molecularly ordered 2-methylimidazole/single-walled carbon nanotubes to form highly porous, electrically conductive composites. *Chem. Sci.* **2019**, *10*, 737−742.
(50) Doherty, C. M.; Knystautas, E.; Buso, D.; Villanova, L.; Konstas, K.; Hill, A. J.; Takahashi, M.; Falcaro, P. Magnetic framework composites for polycyclic aromatic hydrocarbon sequestration. *J. Mater. Chem.* **2012**, *22*, 11470−11474.
(51) Zanchetta, E.; Malfatti, L.; Ricco, R.; Styles, M. J.; Lisi, F.; Coghlan, C. J.; Doonan, C. J.; Hill, A. J.; Brusatin, G.; Falcaro, P. ZnO as an Efficient Nucleating Agent for Rapid, Room Temperature Synthesis and Patterning of Zn-Based Metal-Organic Frameworks. *Chem. Mater.* **2014**, *27*, 690−699.
(52) Liu, Y.; Ghimire, P.; Jaroniec, M. Copper benzene-1,3,5-tricarboxylate (Cu-BTC) metal-organic framework (MOF) and porous carbon composites as efficient carbon dioxide adsorbents. *J. Colloid Interface Sci.* **2019**, *535*, 122−132.
(53) Mao, Y.; Li, G.; Guo, Y.; Li, Z.; Liang, C.; Peng, X.; Lin, Z. Foldable interpenetrated metal-organic frameworks/carbon nanotubes thin film for lithium-sulfur batteries. *Nat. Commun.* **2017**, *8*, 14628.
(54) Ge, L.; Wang, L.; Rudolph, V.; Zhu, Z. Hierarchically structured metal-organic framework/vertically-aligned carbon nanotubes hybrids for CO2 capture. *RSC Adv.* **2013**, *3*, 25360−25366.
(55) Zhu, Q.-L.; Xu, Q. Metal-organic framework composites. *Chem. Soc. Rev.* **2014**, *43*, 5468−5512.

DOI: 10.1021/acsomega.9b00330
ACS Omega 2019, 4, 5275−5282